Research Article

Nano Research
2021, 14(2): 444–449

ISSN 1998-0124 CN 11-5974/O4
https://doi.org/10.1007/s12274-020-3077-1

Rapid room-temperature synthesis of a porphyrinic MOF for encapsulating metal nanoparticles

Huihui He[1], Luyan Li[3], Yang Liu[1], Meruyert Kassymova[3], Dandan Li[2] (✉), Liangliang Zhang[1] (✉), and Hai-Long Jiang[3]

[1] *Frontiers Science Center for Flexible Electronics (FSCFE), Shaanxi Institute of Flexible Electronics (SIFE) & Shaanxi Institute of Biomedical Materials and Engineering (SIBME), Northwestern Polytechnical University (NPU), Xi'an 710072, China*
[2] *Institutes of Physics Science and Information Technology, Anhui University, Hefei 230601, China*
[3] *Hefei National Laboratory for Physical Sciences at the Microscale, Department of Chemistry, University of Science and Technology of China, Hefei 230026, China*

Received: 23 July 2020 / **Revised:** 25 August 2020 / **Accepted:** 26 August 2020

ABSTRACT

While metal nanoparticles (NPs) have shown great promising applications as heterogeneous catalysts, their agglomeration caused by thermodynamic instability is detrimental to the catalytic performance. To tackle this hurdle, we successfully prepared a functional and stable porphyrinic metal-organic framework (MOF), PCN-224-RT, as a host for encapsulating metal nanoparticles by direct stirring at room temperature. As a result, Pt@PCN-224–RT composites with well-dispersed Pt NPs can be constructed by introducing pre-synthesized Pt NPs into the precursor solution of PCN-224-RT. Of note, the rapid and simple stirring method in this work is more in line with the requirements of environmental friendly and industrialization compared with traditional solvothermal methods.

KEYWORDS

metal nanoparticles, room temperature and rapid synthesis, PCN-224, Ostwald ripening

1 Introduction

Metal nanoparticles (MNPs), particularly in small sizes, have attracted great attention due to their advantages in heterogeneous catalysis [1, 2]. However, small MNPs with high surface energy are generally thermodynamically unstable and have a tendency towards agglomeration, which leads to the decrease of catalytic performance [3, 4]. In the past decades, numerous strategies have been proposed to prevent agglomeration of MNPs, among which encapsulation of MNPs into porous materials, such as porous silica, zeolites and metal-organic frameworks (MOFs), could be one of the most effective methods [5–7]. Porous materials can not only benefit the dispersion of MNPs, but also favor the mass transfer of the substrates and products in the catalytic process. Therefore, the encapsulation of MNPs in porous materials for catalysis has been a research hotspot in chemical and material science.

As an emerging porous crystalline material, MOFs possess adjustable pore structures and very high surface areas [8–15]. The unique features of MOFs make them ideal hosts and supports for MNPs, which lead to synergistically enhanced catalysis [16–18]. The general approach to prepare MNPs@MOFs composites is the impregnation of metal precursors into MOFs with various techniques, including solution infiltration, solid grinding, and chemical vapor deposition. After that, the introduced metal precursors are reduced to MNPs by H_2, $NaBH_4$ or other reducing agents [19–21]. In this way, it is possible to adjust the loading position of MNPs relative to MOF particles, the size of MNPs might be controlled by the cavities of MOFs during the reduction process as well. However, both the impregnation and reduction process usually need to be carried out under harsh conditions, which poses a great challenge to the stability of MOF materials. To avoid the damage of MOFs, a post-synthetic encapsulation of MNPs into MOFs was a promising route to establish MNPs@MOFs composites under mild conditions. The pre-synthesized MNPs with fixed size and shape are introduced into the precursor solution of MOFs and then encapsulated directly during the preparation of MOFs [22–24]. Although simple operation and controllable MNPs has been achieved, there are still some issues that need to be addressed. For example, considering the reaction conditions of catalysis, the selected MOF materials, as supports, generally are required to feature high stability. Nevertheless, most of the stable MOF materials, like UiO-66 and MIL-101, were synthesized by solvothermal methods. In order to yield high-quality crystals, the temperatures are usually controlled at around 80–120 °C and typically the reaction time is exceeding 24 h [25, 26], which may negatively affect the embedding of thermally sensitive MNPs. The development of rapid synthesis of MOF materials at a lower temperature (such as room temperature) is a significant countermeasure to overcome these drawbacks.

Based on the above considerations, we thought to prepare the stable MOFs at room temperature to encapsulate classical Pt NPs to avoid the aggregation caused by *in-situ* solvothermal conditions. In order to optimize the catalytic performance

Address correspondence to Dandan Li, chemlidd@163.com; Liangliang Zhang, iamllzhang@nwpu.edu.cn

of MNPs@MOFs composites, a multifunctional and stable porphyrinic MOF, namely PCN-224 ($Zr_6(\mu_3\text{-}OH)_4(OH)_4(TCPP)_6$), was chosen as the target support. The PCN-224, consisting of 6-connected Zr_6 clusters and 4-connected meso-tetra(4-carboxylatophenyl)-porphyrin (TCPP) linkers, possesses outstanding biocompatibility and high catalytic activity [27–29]. Meanwhile, TCPP linkers with both high connectivity and large size contribute to the formation of an open micro/mesoporous structures. Herein, we reported a simple (a directly stirring method) and rapid room-temperature synthesis approach for Pt@PCN-224 composites with well dispersed Pt NPs. In addition, the room-temperature synthetic conditions of PCN-224-RT have been carefully studied. This method introduces an appealing strategy to prepare supports (PCN-224-RT) for dispersing MNPs or other thermo-sensitive materials in a rapid and mild way. From the perspective of environment and industrialization, room temperature syntheses are more advantageous compared with traditional methods.

2 Experimental

2.1 Materials and equipment

All chemicals were obtained from commercial suppliers without further purification unless otherwise mentioned. Powder X-ray diffraction (PXRD) was tested on a PANayltical Empyrean powder X-ray diffractometer equipped with graphite monochromatized Cu Kα radiation (λ = 1.54178 Å) at 40 kV and 40 mA. N_2 adsorption isotherms of PCN-224 series were measured by ASAP-2020 at 77 K. Prior to nitrogen adsorption/desorption measurements, the as-synthesized samples were activated in acetone and then dried in vacuum at 100 °C. After that, the product was dried again by using the "outgas" function for 5 h at 100 °C. Thermogravimetric analysis (TGA) data was collected on a Mettler Toledo thermogravimetric analyzer from 40 to 900 °C. Scanning electron microscopy (SEM) was detected on a S4800 (HITACHI) to show the morphology of the particles. Transmission electron microscopy (TEM) was performed on a JEOL-2010 with electron acceleration energy of 200 kV.

2.2 Preparation of Zr_6 cluster with benzoate capped

The pre-synthesized of Zr_6 cluster was synthesized based on the previous report [30]. Typically, 150 mL of 1-propanol, 7.5 mL of 80 wt.% $Zr(OBu)_4$ in n-butanol and 50 g of benzoic acid were added into a 500 mL flask. The solution was further heated under reflux with stirring for 8 h after being sonicated for 30 min. And then excess solvent was removed by rotary evaporator to obtain a white solid product. Zr_6 cluster can be collected after washing with 1-propanol and dried under vacuum at room temperature. PXRD measurement was performed to check the phase purity of Zr_6 cluster (Fig. S1 in the Electronic Supplementary Material (ESM)).

2.3 Preparation of PCN-224-RT

Typically, 100 mg of as prepared Zr_6 cluster was dissolved in a mixed solution of acetic acid (HOAc, 4 mL) and N,N'-dimethylformamide (DMF, 1 mL) (solution A), while 50 mg TCPP linker was dispersed in 5 mL DMF and dissolved by ultrasonication (solution B). Solution B was added into solution A and kept stirring at room temperature (kept for 0.5, 3, 9 and 12 h, respectively). The products were collected by centrifugation, washed with DMF/EtOH for 3 times to remove the unreacted reactants and then dried in the vacuum.

2.4 Synthesis of Pt@PCN-224-RT

The as-synthesized Pt NPs with uniform size of ~ 3 nm was dispersed in DMF by ultrasonication to form 1 mg·mL^{-1} suspension. Solution B consisted of n mL Pt NPs suspension (n = 1, 3, 5), 5 − n mL DMF and 50 mg TCPP. Solution B was added into solution A under stirring and kept stirring for 12 h at room temperature. The products were collected by centrifugation, washed with DMF/EtOH for 3 times to remove the unreacted reactants and dried in the vacuum.

3 Results and discussion

It is worth noting that mostly room temperature synthesis of Zr_6-based MOFs was obtained via syringe titration at certain speed due to the low solubility of their ligands [31]. Considering the relatively good solubility of TCPP in DMF, we tried to prepare PCN-224 by directly mixing and stirring the metal clusters and ligands, which was easier to operate. The resulting materials (called PCN-224-RT) were obtained by centrifugation, washing with DMF/EtOH to remove unreacted reactants and drying in the vacuum.

As illustrated in Fig. 1(a), the results of PXRD indicate the pure phase of PCN-224-RT. Specifically, the reflection peaks on the PXRD patterns at 2θ = 5.6°, 6.5°, and 7.9° for PCN-224-RT are consistent with those of PCN-224-single crystal data. Furthermore, N_2 adsorption of PCN-224-RT exhibits a permanent porosity with N_2 uptake (768 cm^3·g^{-1}) at 1 atm and 77 K. The Brunauer–Emmett–Teller (BET) surface area of PCN-224-RT can reach up to 2,164 cm^2·g^{-1} and the pore size distribution calculated by DFT method are 12 and 21 Å, which are in good agreement with the reported values (Fig. 1(b)). Moreover, TGA images reveal that the as-synthesized PCN-224-RT possesses similar thermal stability to the reported PCN-224 series, which can stable up to 450 °C (Fig. S2 in the ESM).

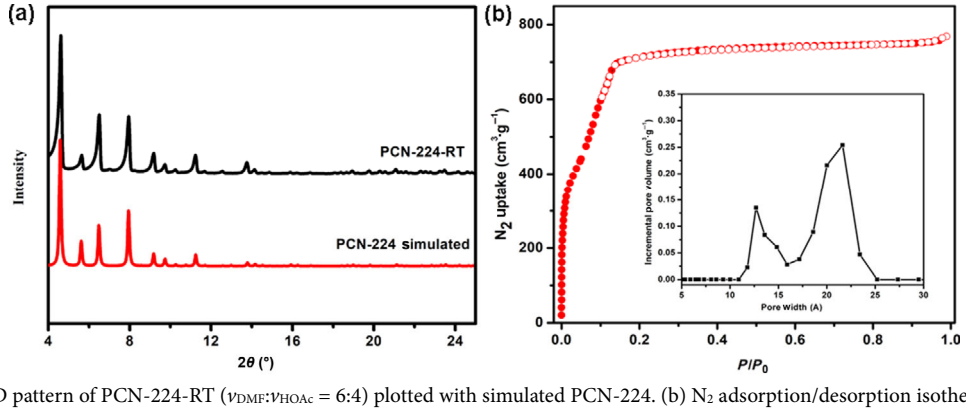

Figure 1 (a) PXRD pattern of PCN-224-RT (v_{DMF}:v_{HOAc} = 6:4) plotted with simulated PCN-224. (b) N_2 adsorption/desorption isotherms of PCN-224-RT (v_{DMF}:v_{HOAc} = 6:4) at 77 K (the inset image is DFT curve).

The synthetic conditions were further explored to satisfy the requirements of the actual production process. Given that modulators play crucial roles in the construction of highly crystalline MOFs through competitive coordination or controlling the deprotonation of ligands [32–34]. By changing the ratio of DMF to HOAc the effect of modulators on the preparation of PCN-224-RT was studied firstly. The proportions of 4:6, 5:5 and 6:4 (v_{DMF}:v_{HOAc}, solution A + B) were selected in the initial attempt and the PXRD results revealed that the target products could be obtained at 5:5 and 6:4 ratios. Next, the proportions were expanded from 6:4 to 10:0. As shown in Fig. 2(a), PCN-224-RT with good quality can be obtained from 6:4 to 9:1 ratios, which further proves the significance of modulating linker in preparation of MOFs. As a result, PCN-224-RT can be obtained in the volume ratio of DMF to HOAc from 9:1 to 5:5. As for the phenomenon that the volume ratio of modulating linker above 1/2 prevented the formation of PCN-224, we attribute it to the fact that the introduction of excessive HOAc reduces the pH value of solution and suppresses the deprotonation of ligands [35].

In addition to the modulators, temperature is also a remarkable factor affecting the synthesis of MOFs. Zr_6 cluster and TCPP can form a variety of MOFs with different topologies under different environments, such as **csq** [36, 37], **shp** [38], **she** [39], **spc** [40] and **ftw** [37, 41]. At the same time, it has also been reported that porphyrinic-based MOF products exhibit different topologies in a synthetic system with temperature variations [30]. Therefore, our attentions were shifted towards reaction temperature. In order to ensure the comprehensiveness of the research, we performed a variable temperature experiment, including 40, 80 and 120 °C, to prepare PCN-224-T. It can be clearly seen from Fig. 2, the change of temperature exhibited a negligible impact on the peak position of the PXRD pattern, which initially demonstrated that no topological changes occur as the temperature variations. The above results unveil that no additional strict temperature control required during MOFs preparation is a significant advantage of our method.

The aforementioned exploration of modulators and temperature promoted us to further explore the impact of reaction time. Generally, traditional solvothermal methods are carried out for more than 24 h, room-temperature synthesis of cluster-based MOFs also requires at least 12 h, which are not conducive to raise efficiency and reduce cost. Considering shorten reaction times caused low yields, we tend to find a balance between yield and reaction time in current systems. Upon fixing the modulator proportion (v_{DMF}:v_{HOAc} = 6:4) and temperature (RT), the reaction time was set as 0.2, 0.5, 3, 9 and 12 h, respectively. Unfortunately, the yield (reaction time: 0.2 h) was too low to obtain sufficient quantities for characterization. In contrast, the resultant product after 0.5 h reaction exhibits a moderate yield (54%). Of note, prolonging the reaction time results in limited increase of yields, for example, the yields are 64% (3 h), 65% (9 h) and 67% (12 h), respectively. All the samples prepared from 0.5 to 9 h were basically characterized by PXRD (Fig. S3 in the ESM). As depicted by N_2 adsorption–desorption isotherm at 77 K, PCN-224-RT-0.5 h, PCN-224-RT-3 h and PCN-224-RT-9 h show similar N_2 adsorption–desorption isotherm and surface areas with PCN-224-single crystal (Figs. S4–S12 in the ESM). According to the density functional theory (DFT)-calculated pore size distribution, the mesoporous defects caused by RT are significantly larger than that of PCN-224 single crystal (Fig. S13 in the ESM). Defective pore structures of MOFs result from disordered displacement or rotation of linkers, and the absence of some Zr_6 center [42]. The resultant PCN-224-RT-t (t = 0.5, 3, 9 and 12 h) can be regarded as a kind of hierarchically porous MOFs.

SEM images were used to reveal the evolution of sphere morphology of the crystals (Fig. 3), which is in agreement with some previous reports [30, 31, 43]. Interestingly, the crystal growth process can be interpreted by Ostwald ripening theory, which reveals that heterogeneous nucleation on the surface is taking place concurrently with crystal growth. Finally,

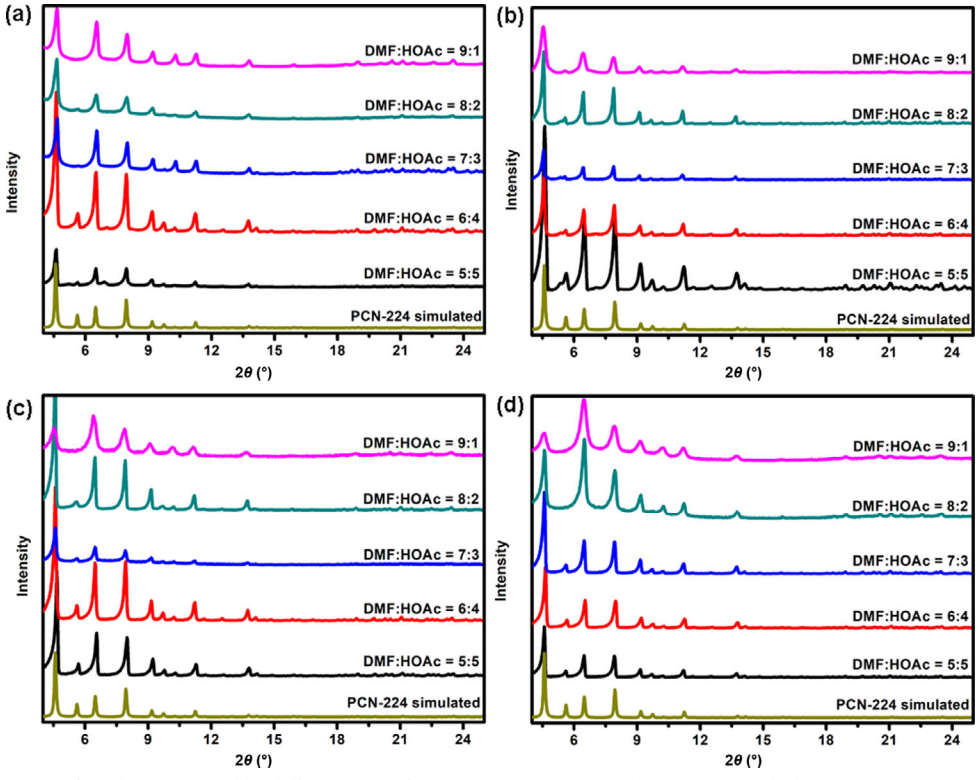

Figure 2 PXRD patterns of products prepared by different ratio of DMF to HOAc at (a) RT, (b) 40, (c) 80 and (d) 120 °C.

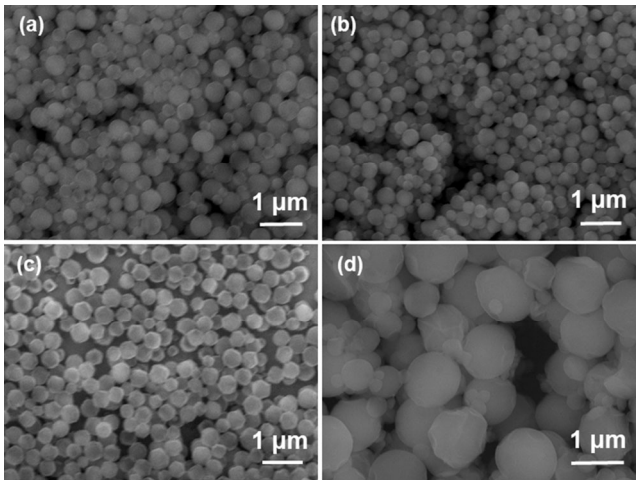

Figure 3 The SEM images of the PCN-224-RT-*t* with different reaction time (a) 0.5, (b) 3, (c) 9 and (d) 12 h, respectively.

accompanied with the disappearance of smaller crystals, the morphologies of the larger crystals evolved from polyhedron into sphere [44].

After comprehensive exploration of the synthetic conditions for PCN-224-RT, we set out to incorporate pre-synthesized Pt NPs into the synthetic system of PCN-224-RT for encapsulation. Pt NPs with uniform size of ~ 3 nm were synthesized [45, 24] and then Pt-1@PCN-224-RT, Pt-3@PCN-224-RT and Pt-5@PCN-224-RT composites were prepared successfully by introducing different amounts of Pt NPs suspension (1, 3 and 5 mL) into the precursor solution of PCN-224-RT. As depicted in Fig. S14 in the ESM, the structure and crystallinity of PCN-224-RT were well maintained and not affected by the encapsulation of Pt NPs. TEM images clearly show that Pt NPs are uniformly dispersed in all of the three MOF composites, suggesting the feasibility of our strategy (Fig. 4). With the increase of Pt NPs in the synthetic system, the dispersion density of Pt NPs within PCN-224-RT gradually enhanced and the average size of the composites decreased (Fig. S15 in the ESM). Moreover, obviously morphology change can be observed for Pt-5@PCN-224-RT composites when the introduced Pt NPs increases to 5 mg. That is mainly attributed to the fact that excessive introduction of MNPs will affect the crystal nucleation and growth. As reported, the surfactant and the precursor of MOF have strong interaction/affinity, which will inhibit the process of crystal nucleation and growth, thus modulate crystal size [46]. Moreover, our universality approach can be extended into other MNPs, such as Pd nanocubes with different sizes (Fig. S16 in the ESM). Notably, this rapid room-temperature synthesis method not only makes MNPs encapsulation feasible over PCN-224-RT, but also endows MNPs@PCN-224-RT with interesting photocatalytic properties (light-driven $^1O_2$ generation ability of Pt-3@PCN-224-RT is illustrated in Fig. 5). PXRD of Pt-3@PCN-224-RT after photocatalytic reaction demonstrated the stability of the composites (Fig. S17 in the ESM). In future endeavor, the catalytic performance of MNPs@PCN-224-RT will be systematically studied.

4 Conclusions

In summary, a series of PCN-224-RT were successfully prepared as support/host to disperse thermally sensitive Pt NPs via a directly stirring method at room temperature. This method can construct the target PCN-224 in a wide range of temperature (RT to 120 °C) and modulating linker ratios (5:5–9:1, v_{DMF}:v_{HOAc}), such mild preparation conditions are suitable for large-scale preparation. By this rapid approach, PCN-224-RT with high yields can be obtained within half an hour, which is beneficial to reduce the cost. Moreover, MNPs@PCN-224-RT, promising photosensitive catalysts, were successfully prepared with well dispersed MNPs by introducing pre-synthesized MNPs into the precursor solution of PCN-224-RT. The successful preparation of the PCN-224-RT composites provides a new dispersed method for the thermodynamically unstable materials

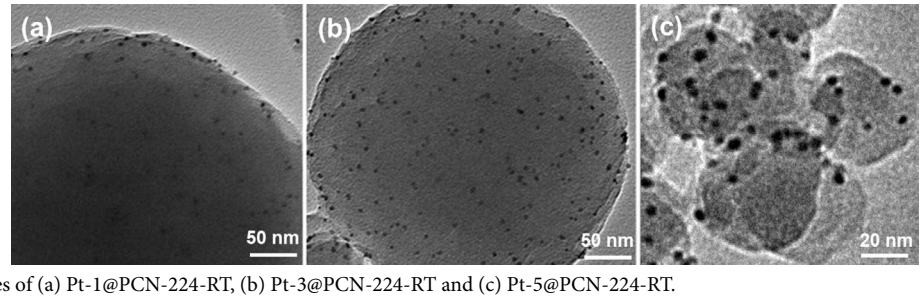

Figure 4 TEM images of (a) Pt-1@PCN-224-RT, (b) Pt-3@PCN-224-RT and (c) Pt-5@PCN-224-RT.

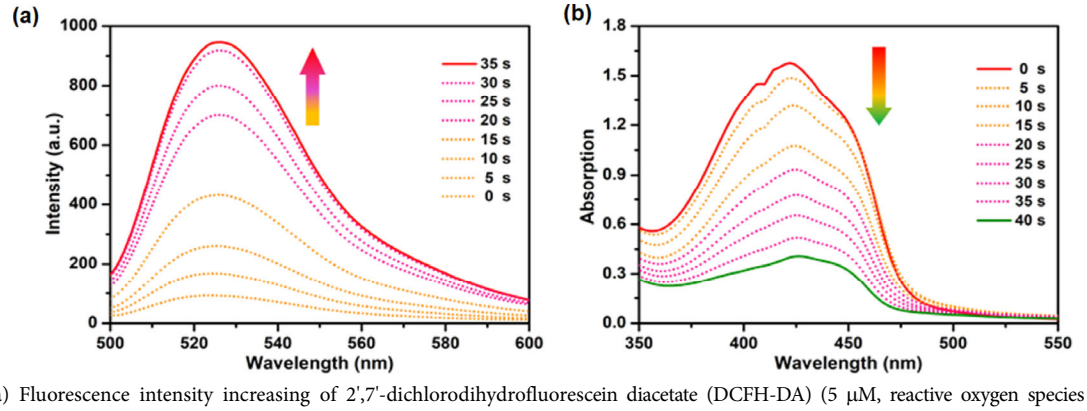

Figure 5 (a) Fluorescence intensity increasing of 2',7'-dichlorodihydrofluorescein diacetate (DCFH-DA) (5 μM, reactive oxygen species indicator) in Pt-3@PCN-224-RT suspension (100 μg·mL^{-1}) under visible-light irradiation. (b) Gradual absorbance reduction of 1,3-diphenylisobenzofuran (DPBF) (0.1 mM, $^1O_2$ indicator) in Pt-3@PCN-224-RT suspension (100 μg·mL^{-1}) induced by visible-light irradiation.

and opens a new avenue to the growth, assembly and morphology control of nanoscale MOF composites.

Acknowledgements

This work was supported by the National Natural Science Foundation of China (Nos. 21701187 and 21701160), Natural Science Basic Research Program of Shaanxi (No. 2020JQ-142), and the Fundamental Research Funds for the Central Universities (No. 31020180QD115).

Electronic Supplementary Material: Supplementary material (details for synthesis and characterization of Zr_6 clusters, PCN-224-RT, N_2 uptake, Pt NPs and Pd nanocubes, respectively) is available in the online version of this article at https://doi.org/10.1007/s12274-020-3077-1.

References

[1] Choi, K. M.; Kim, D.; Rungtaweevoranit, B.; Trickett, C. A.; Barmanbek, J. T. D.; Alshammari, A. S.; Yang, P. D.; Yaghi, O. M. Plasmon-enhanced photocatalytic CO_2 conversion within metal-organic frameworks under visible light. *J. Am. Chem. Soc.* **2017**, *139*, 356–362.

[2] Zhan, W. W.; Zhu, Q. L.; Xu, Q. Dehydrogenation of ammonia borane by metal nanoparticle catalysts. *ACS Catal.* **2016**, *6*, 6892–6905.

[3] Li, Z.; Ji, S. F.; Liu, Y. W.; Cao, X.; Tian, S. B.; Chen, Y. J.; Niu, Z. Q.; Li, Y. D. Well-defined materials for heterogeneous catalysis: From nanoparticles to isolated single-atom sites. *Chem. Rev.* **2020**, *120*, 623–682.

[4] Chen, Y.; Yang, X. C.; Kitta, M.; Xu, Q. Monodispersed Pt nanoparticles on reduced graphene oxide by a non-noble metal sacrificial approach for hydrolytic dehydrogenation of ammonia borane. *Nano Res.* **2017**, *10*, 3811–3816.

[5] White, R. J.; Luque, R.; Budarin, V. L.; Clark, J. H.; Macquarrie, D. J. Supported metal nanoparticles on porous materials. Methods and applications. *Chem. Soc. Rev.* **2009**, *38*, 481–494.

[6] Goel, S.; Wu, Z. J.; Zones, S. I.; Iglesia, E. Synthesis and catalytic properties of metal clusters encapsulated within small-pore (SOD, GIS, ANA) zeolites. *J. Am. Chem. Soc.* **2012**, *134*, 17688–17695.

[7] Wang, B. Q.; Liu, W. X.; Zhang, W. N.; Liu, J. F. Nanoparticles@nanoscale metal-organic framework composites as highly efficient heterogeneous catalysts for size- and shape-selective reactions. *Nano Res.* **2017**, *10*, 3826–3835.

[8] Shi, Z. L.; Tao, Y.; Wu, J. S.; Zhang, C. Z.; He, H. L.; Long, L. L.; Lee, Y.; Li, T.; Zhang, Y. B. Robust metal-triazolate frameworks for CO_2 capture from flue gas. *J. Am. Chem. Soc.* **2020**, *142*, 2750–2754.

[9] Cho, H. S.; Yang, J. J.; Gong, X.; Zhang, Y. B.; Momma, K.; Weckhuysen, B. M.; Deng, H. X.; Kang, J. K.; Yaghi, O. M.; Terasaki, O. Isotherms of individual pores by gas adsorption crystallography. *Nat. Chem.* **2019**, *11*, 562–570.

[10] Hu, P.; Zhuang, J.; Chou, L. Y.; Lee, H. K.; Ling, X. Y.; Chuang, Y. C.; Tsung, C. K. Surfactant-directed atomic to mesoscale alignment: Metal nanocrystals encased individually in single-crystalline porous nanostructures. *J. Am. Chem. Soc.* **2014**, *136*, 10561–10564.

[11] Wang, L. Y.; Xu, H.; Gao, J. K.; Yao, J. M.; Zhang, Q. C. Recent progress in metal-organic frameworks-based hydrogels and aerogels and their applications. *Coord. Chem. Rev.* **2019**, *398*, 213016.

[12] Li, W. H.; Ding, K.; Tian, H. R.; Yao, M. S.; Nath, B.; Deng, W. H.; Wang, Y. B.; Xu, G. Conductive metal-organic framework nanowire array electrodes for high-performance solid-state supercapacitors. *Adv. Funct. Mater.* **2017**, *27*, 1702067.

[13] Zhang, Q.; Su, J.; Feng, D. W.; Wei, Z. W.; Zou, X. D.; Zhou, H. C. Piezofluorochromic metal-organic framework: A microscissor lift. *J. Am. Chem. Soc.* **2015**, *137*, 10064–10067.

[14] Li, N.; Liu, J.; Liu, J. J.; Dong, L. Z.; Xin, Z. F.; Teng, Y. L.; Lan, Y. Q. Adenine components in biomimetic metal-organic frameworks for efficient CO_2 photoconversion. *Angew. Chem., Int. Ed.* **2019**, *58*, 5226–5231.

[15] Jiao, L.; Seow, J. Y. R.; Skinner, W. S.; Wang, Z. U.; Jiang, H. L. Metal-organic frameworks: Structures and functional applications. *Mater. Today* **2019**, *27*, 43–68.

[16] Liu, J. W.; Chen, L. F.; Cui, H.; Zhang, J. Y.; Zhang, L.; Su, C. Y. Applications of metal-organic frameworks in heterogeneous supramolecular catalysis. *Chem. Soc. Rev.* **2014**, *43*, 6011–6061.

[17] Huang, Y. B.; Liang, J.; Wang, X. S.; Cao, R. Multifunctional metal-organic framework catalysts: Synergistic catalysis and tandem reactions. *Chem. Soc. Rev.* **2017**, *46*, 126–157.

[18] Yang, Q. H.; Xu, Q.; Jiang, H. L. Metal-organic frameworks meet metal nanoparticles: Synergistic effect for enhanced catalysis. *Chem. Soc. Rev.* **2017**, *46*, 4774–4808.

[19] Chen, Y. Z.; Zhou, Y. X.; Wang, H. W.; Lu, J. L.; Uchida, T.; Xu, Q.; Yu, S. H.; Jiang, H. L. Multifunctional PdAg@MIL-101 for one-pot cascade reactions: Combination of host-guest cooperation and bimetallic synergy in catalysis. *ACS Catal.* **2015**, *5*, 2062–2069.

[20] Chen, Y. Z.; Gu, B. C.; Uchida, T.; Liu, J. D.; Liu, X. C.; Ye, B. J.; Xu, Q.; Jiang, H. L. Location determination of metal nanoparticles relative to a metal-organic framework. *Nat. Commun.* **2019**, *10*, 3462.

[21] Chen, L. Y.; Chen, H. R.; Luque, R.; Li, Y. W. Metal-organic framework encapsulated Pd nanoparticles: Towards advanced heterogeneous catalysts. *Chem. Sci.* **2014**, *5*, 3708–3714.

[22] Liu, Y.; Shen, Y.; Zhang, W. N.; Weng, J. N.; Zhao, M. T.; Zhu, T. S.; Chi, Y. R.; Yang, Y. H.; Zhang, H.; Huo, F. W. Engineering channels of metal-organic frameworks to enhance catalytic selectivity. *Chem. Commun.* **2019**, *55*, 11770–11773.

[23] Lu, G.; Li, S. Z.; Guo, Z.; Farha, O. K.; Hauser, B. G.; Qi, X. Y.; Wang, Y.; Wang, X.; Han, S. Y.; Liu, X. G. et al. Imparting functionality to a metal-organic framework material by controlled nanoparticle encapsulation. *Nat. Chem.* **2012**, *4*, 310–316.

[24] Xiao, J. D.; Shang, Q. C.; Xiong, Y. J.; Zhang, Q.; Luo, Y.; Yu, S. H.; Jiang, H. L. Boosting photocatalytic hydrogen production of a metal-organic framework decorated with platinum nanoparticles: The platinum location matters. *Angew. Chem., Int. Ed.* **2016**, *55*, 9389–9393

[25] Cavka, J. H.; Jakobsen, S.; Olsbye, U.; Guillou, N.; Lamberti, C.; Bordiga, S.; Lillerud, K. P. A new zirconium inorganic building brick forming metal organic frameworks with exceptional stability. *J. Am. Chem. Soc.* **2008**, *130*, 13850–13851.

[26] Lebedev, O. I.; Millange, F.; Serre, C.; Van Tendeloo, G.; Férey, G. First direct imaging of giant pores of the metal-organic framework MIL-101. *Chem. Mater.* **2005**, *17*, 6525–6527.

[27] Feng, D. W.; Chung, W. C.; Wei, Z. W.; Gu, Z. Y.; Jiang, H. L.; Chen, Y. P.; Darensbourg, D. J.; Zhou, H. C. Construction of ultrastable porphyrin Zr metal-organic frameworks through linker elimination. *J. Am. Chem. Soc.* **2013**, *135*, 17105–17110.

[28] Tian, S. F.; Chen, S. D.; Ren, X. T.; Hu, Y. Q.; Hu, H. Y.; Sun, J. J.; Bai, F. An efficient visible-light photocatalyst for CO_2 reduction fabricated by cobalt porphyrin and graphitic carbon nitride via covalent bonding. *Nano Res.* **2020**, *13*, 2665–2672.

[29] Tian, S. F.; Chen, S. D.; Ren, X. T.; Cao, R. H.; Hu, H. Y.; Bai, F. Bottom-up fabrication of graphitic carbon nitride nanosheets modified with porphyrin via covalent bonding for photocatalytic H_2 evolution. *Nano Res.* **2019**, *12*, 3109–3115.

[30] Gong, X. Y.; Noh, H.; Gianneschi, N. C.; Farha, O. K. Interrogating kinetic versus thermodynamic topologies of metal-organic frameworks via combined transmission electron microscopy and X-ray diffraction analysis. *J. Am. Chem. Soc.* **2019**, *141*, 6146–6151.

[31] Noh, H.; Kung, C. W.; Islamoglu, T.; Peters, A. W.; Liao, Y. J.; Li, P.; Garibay, S. J.; Zhang, X.; DeStefano, M. R.; Hupp, J. T. et al. Room temperature synthesis of an 8-connected Zr-based metal-organic framework for top-down nanoparticle encapsulation. *Chem. Mater.* **2018**, *30*, 2193–2197.

[32] Zhang, L. L.; Yuan, S.; Fan, W. D.; Pang, J. D.; Li, F. G.; Guo, B. B.; Zhang, P.; Sun, D. F.; Zhou, H. C. Cooperative sieving and functionalization of Zr metal-organic frameworks through insertion and post-modification of auxiliary linkers. *ACS Appl. Mater. Interfaces* **2019**, *11*, 22390–22397.

[33] Shaikh, S. M.; Usov, P. M.; Zhu, J.; Cai, M.; Alatis, J.; Morris, A. J. Synthesis and defect characterization of phase-pure Zr-MOFs based on meso-tetracarboxyphenylporphyrin. *Inorg. Chem.* **2019**, *58*, 5145–5153.

[34] Xu, H. Q.; Wang, K. C.; Ding, M. L.; Feng, D. W.; Jiang, H. L.; Zhou, H. C. Seed-mediated synthesis of metal-organic frameworks. *J. Am. Chem. Soc.* **2016**, *138*, 5316–5320.
[35] Yuan, S.; Feng, L.; Wang, K. C.; Pang, J. D.; Bosch, M.; Lollar, C.; Sun, Y. J.; Qin, J. S.; Yang, X. Y.; Zhang, P. et al. Stable metal-organic frameworks: Design, synthesis, and applications. *Adv. Mater.* **2018**, *30*, 1704303.
[36] Feng, D. W.; Gu, Z. Y.; Li, J. R.; Jiang, H. L.; Wei, Z. W.; Zhou, H. C. Zirconium-metalloporphyrin PCN-222: Mesoporous metal-organic frameworks with ultrahigh stability as biomimetic catalysts. *Angew. Chem., Int. Ed.* **2012**, *51*, 10307–10310.
[37] Morris, W.; Volosskiy, B.; Demir, S.; Gándara, F.; McGrier, P. L.; Furukawa, H.; Cascio, D.; Stoddart, J. F.; Yaghi, O. M. Synthesis, structure, and metalation of two new highly porous zirconium metal-organic frameworks. *Inorg. Chem.* **2012**, *51*, 6443–6445.
[38] Feng, D. W.; Gu, Z. Y.; Chen, Y. P.; Park, J.; Wei, Z. W.; Sun, Y. J.; Bosch, M.; Yuan, S.; Zhou, H. C. A highly stable porphyrinic zirconium metal-organic framework with shp-a topology. *J. Am. Chem. Soc.* **2014**, *136*, 17714–17717.
[39] Zhang, L. L.; Yuan, S.; Feng, L.; Guo, B. B.; Qin, J. S.; Xu, B.; Lollar, C.; Sun, D. F.; Zhou, H. C. Pore-environment engineering with multiple metal sites in rare-earth porphyrinic metal-organic frameworks. *Angew. Chem., Int. Ed.* **2018**, *57*, 5095–5099.
[40] Jiang, H. L.; Feng, D. W.; Wang, K. C.; Gu, Z. Y.; Wei, Z. W.; Chen, Y. P.; Zhou, H. C. An exceptionally stable, porphyrinic Zr metal-organic framework exhibiting pH-dependent fluorescence. *J. Am. Chem. Soc.* **2013**, *135*, 13934–13938.
[41] Feng, D. W.; Jiang, H. L.; Chen, Y. P.; Gu, Z. Y.; Wei, Z. W.; Zhou, H. C. Metal-organic frameworks based on previously unknown Zr_8/Hf_8 cubic clusters. *Inorg. Chem.* **2013**, *52*, 12661–12667.
[42] Epley, C. C.; Love, M. D.; Morris, A. J. Characterizing defects in a UiO-AZB metal-organic framework. *Inorg. Chem.* **2017**, *56*, 13777–13784.
[43] DeStefano, M. R.; Islamoglu, T.; Garibay, S. J.; Hupp, J. T.; Farha, O. K. Room-temperature synthesis of UiO-66 and thermal modulation of densities of defect sites. *Chem. Mater.* **2017**, *29*, 1357–1361.
[44] Van Vleet, M. J.; Weng, T. T.; Li, X. Y.; Schmidt, J. R. *In situ*, time-resolved, and mechanistic studies of metal-organic framework nucleation and growth. *Chem. Rev.* **2018**, *118*, 3681–3721.
[45] Chen, Y. Z.; Wang, Z. U.; Wang, H. W.; Lu, J. L.; Yu, S. H.; Jiang, H. L. Singlet oxygen-engaged selective photo-oxidation over Pt nanocrystals/porphyrinic MOF: The roles of photothermal effect and Pt electronic state. *J. Am. Chem. Soc.* **2017**, *139*, 2035–2044.
[46] Li, H.; Meng, F. C.; Zhang, S. Y.; Wang, L. G.; Li, M.; Ma, L.; Zhang, W. N.; Zhang, W. L.; Yang, Z. H.; Wu, T. P. et al. Crystal-growth-dominated fabrication of metal-organic frameworks with orderly distributed hierarchical porosity. *Angew. Chem., Int. Ed.* **2020**, *59*, 2457–2464.